Robotica (2015) volume 33, pp. 1948–1957. © Cambridge University Press 2014
doi:10.1017/S0263574714000861

Cartesian workspace optimization of Tricept parallel manipulator with machining application

M. A. Hosseini†* and H. M. Daniali‡

†*Department of Mechanical Engineering, University of Mazandaran, Babolsar, Iran*
‡*Department of Mechanical Engineering, Babol University of Technology, Babol, Iran*

(Accepted March 7, 2014. First published online: May 14, 2014)

SUMMARY
In this research work, the maximum Cartesian workspace of a Tricept parallel robot with two rotational and one translational degrees of freedom was investigated. Generally, the Cartesian workspace identifies the maximum size of a work-piece, specifying its cubic x, y and z dimensions, on which the milling machine could perform operations. However, the workspace of a robot can be considered in its task space, such as $\psi \times \theta \times z$ for the Tricept Parallel Kinematic Mechanism (PKM). A novel homogeneous Jacobian matrix which transforms joint space velocity vector into end-effector Cartesian velocity vector has been generated named as a Cartesian Jacobian matrix. Using the indices derived from the homogeneous Cartesian Jacobian matrix, i.e. the maximum singular values and local conditioning indices, the manipulator is designed to reach the Cartesian workspace with rapid positioning rates as well as with singularity avoidance.

KEYWORDS: Cartesian workspace; Rapid positioning; Homogenized Cartesian Jacobian matrix; Parallel robot.

1. Introduction

Parallel robots have significant advantages over their serial counterparts, which drew the attention of researchers and manufacturers throughout the last two decades. These advantages, such as low inertia, high stiffness, high precision, and high load carrying capacity,[1,2] made them powerful tools in machining, simulating, and pick-and-place tasks.

Complex degrees of freedom (DoF) robots are those that have both rotational and translational DoFs.[3] This leads to an inhomogeneity of Jacobian matrix entries, which makes it a problem to use performance indices such as condition number and manipulability.[4] To resolve this problem, Salisbury and Craig[5] introduced the ratio between maximum and minimum singular values as the condition number in Euclidean norm. The inverse of the Euclidean condition number is defined as the Local Condition Index (LCI) which varies from 0 to 1. Condition number has been used for measuring robot conditions and relative error analysis.[6–11] Further, Gosselin and Angeles[6] introduced the average of condition index throughout the workspace as global condition index (GCI). This index reveals the tendency of the robot structure towards isotropy. Other researchers[8–11] have applied these indices for optimizing the structure of the robot and to achieve other desired objectives, such as dexterity, isotropy, and accurate robot positioning and orientation. Ranjbaran *et al.*[12] resolved this inconsistency by defining a coefficient named as characteristic length with the dimension of length. In the suggested method, entries with the dimension of length, are divided by the mentioned coefficient, thus the homogeneous Jacobian with new dimensionless entries is developed. Ma and Angeles[13] introduced another ratio called natural length and used it for design optimization. Chablat *et al.*[14] used characteristic length to determine the design parameter of a planar parallel mechanism with Prismatic–Revolute–Revolute (P-R-R) chains to have an isotropic condition. Gosselin[15] introduced a method for formulating dimensionally homogeneous Jacobian matrix for a planar mechanism with one rotational and two translational DoFs. This Jacobian matrix relates the actuator velocities to the

* Corresponding author. E-mail: ma.hosseini@umz.ac.ir

https://doi.org/10.1017/S0263574714000861 Published online by Cambridge University Press

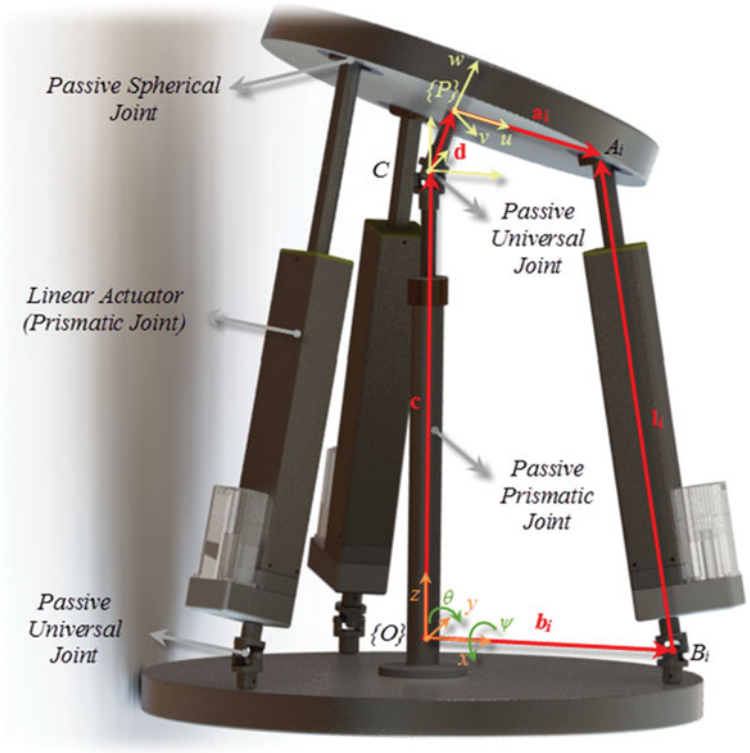


Fig. 1. Tricept structure and geometric model.

velocities of the x and y coordinates of two points on a moving platform. Kim and Ryu[16] furthered this work by using the velocities of three points on a moving platform to develop a dimensionally homogeneous Jacobian matrix. Pond and Carretero[17] furthered this method again by using three independent coordinates of three points on a moving platform. Moreover, Angeles[18] introduced engineering characteristic length for a rigid body transformation matrix to make it homogeneous. Mansouri[19] used the power transition concept to make the Jacobian homogeneous. Hosseini and Daniali[20] suggested using weighted factor methods to make Jacobian matrix homogeneous. Hosseini *et al.*[10,11] used genetic algorithms (GA) to optimize workspace shape and size of Tricept parallel robot in which the DoF of the manipulator was considered by an elevation and two rotations. Here, considering the x-y-z coordinates of the end-effector (EE), the workspace of the robot has been determined through the Cartesian coordinate system. Driving the kinematics equations with respect to time, the Cartesian velocity vector of the EE has been mapped into the joint space velocity vector by a novel homogenized Jacobian matrix, named as homogeneous Cartesian Jacobian matrix. We achieve the optimal structure with the maximum applicable volume of workspace with bounding the associate singular values and LCIs with GA method.

2. Tricept Robot

A Tricept robot, as depicted in Fig. 1, has two rotational and one translational DoFs.[21] The manipulator has three actuated limbs which connect the base to the moving platform. Each of these limbs, i.e. A_iB_i, consists of a Spherical–Prismatic–Spherical (SPS) kinematic chain, where only the prismatic joint is actuated. Alternatively, one of the spherical joints can be replaced by a universal joint. Moreover, a passive prismatic-universal (PU) limb, i.e. OC, connects the center of the moving platform to the base. We attach frames $\{P\ (uvw)\}$ and $\{O\ (xyz)\}$ to the moving and base platforms, respectively. When the moving platform is parallel to the base, the two revolute axes of the universal joints of the center passive leg are parallel with the base frame's x- and y-axes, respectively.

Siciliano[22] studied the kinematics and manipulability of Tricept. Pond and Carretero[17] formulated its square dimensionally homogeneous Jacobian matrices based on three independent coordinates of

https://doi.org/10.1017/S0263574714000861 Published online by Cambridge University Press

three nodes of the moving platform. Architectural optimization of Tricept was studied by Zhang and Gosselin.[23] They used GA method to optimize the stiffness and moving platform accuracy. Here, we use the weighted factor method and analytical method and a numerical search to calculate the workspace. We use the GA method to optimize the dexterous Cartesian workspace of Tricept robot.

2.1. Velocity analysis

The loop closure equation for the *i*th leg can be written as

$$\mathbf{c} + \mathbf{R}(\mathbf{a}_i + \mathbf{d}) = b_i \mathbf{n}_{bi} + l_i \mathbf{n}_{li}, \tag{1}$$

where $\mathbf{c}$ and $\mathbf{d}$ are the vectors from O to C and C to P, respectively. The upper part of the middle link, i.e. $\mathbf{d}$, plays an important role on the workspace volume and shape.[10,11] Moreover, $\mathbf{R}$ is a rotation matrix carrying frame $\{P\}$ into an orientation coincident with that of frame $\{O\}$; $\mathbf{a}_i$ is the position vector from P to A_i in frame $\{P\}$; $\mathbf{b}_i$ is the position vector of point B_i in the global frame; $\mathbf{n}_{bi}$ and $\mathbf{n}_{li}$ are the unit vectors showing the directions of vectors $\mathbf{b}_i$ and $\mathbf{l}_i$, respectively.

Taking the first time derivative of Eq. (1) yields

$$\dot{\boldsymbol{c}} + \boldsymbol{\omega}_p \times (\mathbf{R}(\mathbf{a}_i + \mathbf{d})) = \dot{l}_i \mathbf{n}_{li} + \boldsymbol{\omega}_{li} \times l_i \mathbf{n}_{li}, \tag{2}$$

where $\boldsymbol{\omega}_p$ and $\boldsymbol{\omega}_{li}$ are the angular velocity vectors of the EE and *i*th limb, respectively. Pre-multiplying both sides of Eq. (2) by ${\mathbf{n}_{li}}^T$, upon simplifications leads to:

$$\mathbf{n}_{li}^{\mathrm{T}} \dot{\boldsymbol{c}} + \mathbf{n}_{li}^{\mathrm{T}} \boldsymbol{\omega}_p \times (\mathbf{R}(\mathbf{a}_i + \mathbf{d})) = \dot{l}_i. \tag{3}$$

Written Eq. (4), for $i = 1 \ldots 3$, yields

$$\mathbf{J}\dot{\mathbf{x}} = \dot{\mathbf{q}}, \tag{4}$$

where $\dot{\mathbf{x}}$ is the three-dimensional twist vector of the EE, $\dot{\mathbf{q}}$ is the three-dimensional actuator velocity vector, and $\mathbf{J}$ is the Jacobian matrix, namely,

$$\dot{\mathbf{x}} = [\, \dot{\psi} \quad \dot{\theta} \quad \dot{c} \,]^{\mathrm{T}}, \tag{5}$$

$$\dot{\mathbf{q}} = [\, \dot{l}_1 \quad \dot{l}_2 \quad \dot{l}_3 \,]^{\mathrm{T}}, \tag{6}$$

$$\mathbf{J} = \begin{bmatrix} (\mathbf{R}(\mathbf{a}_1 + \mathbf{d}) \times \mathbf{n}_{l1})_x & (\mathbf{R}(\mathbf{a}_1 + \mathbf{d}) \times \mathbf{n}_{l1})_y & n_{l1z} \\ (\mathbf{R}(\mathbf{a}_2 + \mathbf{d}) \times \mathbf{n}_{l2})_x & (\mathbf{R}(\mathbf{a}_2 + \mathbf{d}) \times \mathbf{n}_{l2})_y & n_{l2z} \\ (\mathbf{R}(\mathbf{a}_3 + \mathbf{d}) \times \mathbf{n}_{l3})_x & (\mathbf{R}(\mathbf{a}_3 + \mathbf{d}) \times \mathbf{n}_{l3})_y & n_{l3z} \end{bmatrix}. \tag{7}$$

In Eq. (5) the linear velocity of the EE is the same as the velocity of the passive prismatic joint.

3. Workspace Analysis

In this section, we study the workspace of a Tricept manipulator numerically by applying the inverse kinematic solution and bounding the condition number for singularity avoidance. Here, we use a different approach than those reported in refs. [16, 17, 24 and 25] in which forward kinematic were used.

3.1. Algorithm

In order to generate the workspace of a Tricept parallel manipulator, we divide the three-dimensional ψ–θ–Z workspace of the moving platform into a series of sub-workspaces that are parallel to ψ–θ plane. Then a numerical searching method, which was introduced in refs. [16, 17], is adopted here to determine the boundaries of the sub-workspaces. Finally, the volume of workspace is calculated quantitatively.

In the particular sub-workspace at elevation Z_i (within the workspace), when determining the boundary of a sub-workspace one may find trajectories formed by the end of polar vector ρ_i rotating about z axis from 0 to 2π, see Fig. 2. When the boundary point in the direction of ρ_i is found as P_i

https://doi.org/10.1017/S0263574714000861 Published online by Cambridge University Press

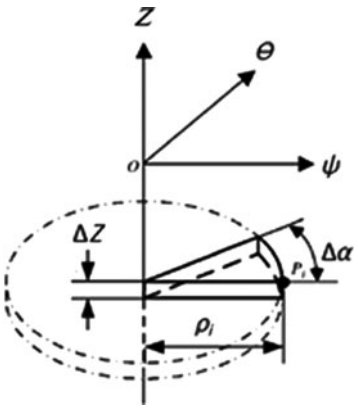


Fig. 2. Boundary points of a sub-workspace.

Table I. Geometric constraints of the Tricept manipulator.

Actuator length (mm)	ζ (deg)	d (mm)	r_b (mm)	r_a (mm)
400–750	$\pm$ 60	0–200	300–500	200–300

(ρCosα, ρSinα, Z_i); where ρ_i is the distance between Z_i and P_i, α will be increased by $\Delta\alpha$, and the next point will be found, similarly. The determination of point P_i is based on the inverse kinematics of the Tricept. When searching the next boundary point P_{i+1}, we set the initial value of ρ_{i+1} as ρ_i, and judge whether point P_{i+1} is in the range of workspace; if yes, then increase ρ_{i+1}, if not, then decrease ρ_{i+1} until point P_{i+1} is on the boundary of the workspace. Once the boundary points in the sub-workspace are all searched out, Z_i will be decreased by ΔZ, and the new searching will be performed again. Moreover, when α is increased by $\Delta\alpha$, the unit volume of the corresponding workspace can be expressed approximately as

$$dV = \frac{\Delta\alpha}{2\pi}\pi\rho_i^2\Delta Z. \tag{8}$$

Therefore, the volume of the workspace can be calculated as

$$V = \sum_{Z_i=Z_{\min}}^{Z_{\max}} \sum_{\alpha=0}^{2\pi} \frac{1}{2}\rho_i^2\Delta\alpha\Delta Z. \tag{9}$$

3.2. Geometric constraints

These constraints include the actuators lengths (l) and the spherical and universal joint limitations. It is simple to calculate the cone angle of joints (ζ) by using the geometric constraints and kinematics relations. The geometric constraints of the Tricept are given in Table I.

3.3. Design constraints

In order to guarantee the workspace to be effective, constraints on the dexterity indices are introduced to characterize the quality of the workspace. Condition number is quite often used as an index to describe the dexterity of a robot and the distance of a pose from a singularity. The condition number also measures the magnitude of the relative error of the wrench introduced by the relative error in joint torques. It reflects the sensitivity of the wrench due to joint torque error. Similarly, the use of minimum allowable singular value restricts the workspace to poses where the manipulator moves at a minimum allowable speed. Here, we optimize Tricept for dexterity measures, namely, the inverse of condition number as a LCI and minimum singular value (MSV) of the Jacobian.

https://doi.org/10.1017/S0263574714000861 Published online by Cambridge University Press

Table II. The case study: Tricept parameters.

Actuator stroke (mm)	c stroke (mm)	d (mm)	r_b (mm)	r_a (mm)
400–750	400–200	200	300	200

3.4. Cartesian workspace

Considering Fig. 1, the EE Cartesian coordinate can be defined as a function of two rotation angles and one elevating coordinate, i.e. ψ, θ, and Z.

$$\mathbf{x_c} = \begin{bmatrix} X \\ Y \\ Z \end{bmatrix} = \begin{bmatrix} C\theta & S\psi S\theta & C\psi S\theta \\ 0 & C\psi & -S\psi \\ -S\theta & C\theta S\psi & C\theta C\psi \end{bmatrix} \begin{bmatrix} 0 \\ 0 \\ d \end{bmatrix} + \begin{bmatrix} 0 \\ 0 \\ c \end{bmatrix}. \tag{10}$$

The above equation can be rewritten as follows:

$$\mathbf{x_c} = \begin{bmatrix} dC\psi S\theta \\ -dS\psi \\ c + dC\theta C\psi \end{bmatrix}. \tag{11}$$

Accordingly, the Cartesian velocity vector, $\dot{\mathbf{x}}_\mathbf{c}$ can be identified as follows:

$$\dot{\mathbf{x}}_\mathbf{c} = \begin{bmatrix} \dot{X} & \dot{Y} & \dot{Z} \end{bmatrix}^T = \widehat{\mathbf{J}}\dot{\mathbf{x}}, \tag{12}$$

in which

$$\widehat{\mathbf{J}} = \begin{bmatrix} -dS\theta S\psi & dC\psi C\theta & 0 \\ -dC\psi & 0 & 0 \\ -dC\theta S\psi & -dS\theta C\psi & 1 \end{bmatrix}. \tag{13}$$

In the light of Eqs. (5) and (7), the Cartesian Jacobian matrix can be defined as follows:

$$\mathbf{J_c} = \mathbf{J}\widehat{\mathbf{J}}^{-1}, \tag{14}$$

which corresponds the Cartesian velocity vector into the joint velocity vector as Eq. (15).

$$\mathbf{J_c}\dot{\mathbf{x}}_\mathbf{c} = \dot{\mathbf{q}} \tag{15}$$

Thus, the Cartesian Jacobian matrix is homogenized and the performance indices could be derived accordingly. Using the same search algorithm method, as mentioned earlier, the boundary points of the Cartesian workspace can be determined.

4. Case Study

Considering a mechanism with the parameters as depicted in Table II, as the case study, and the search algorithm, the Cartesian workspace is calculated. This workspace is depicted in Fig. 3.

4.1. Maximum Cartesian workspace

Using GA toolbox in Matlab software and considering the objective function and constraints as follows:

$$\begin{aligned} &V^* = Max(V(r_a, r_b, d)) \\ &\textit{Subject to:} \\ &0.2 < r_a < 0.3, 0.3 < r_b < 0.5, 0.02 < d < 0.7. \end{aligned} \tag{16}$$

https://doi.org/10.1017/S0263574714000861 Published online by Cambridge University Press

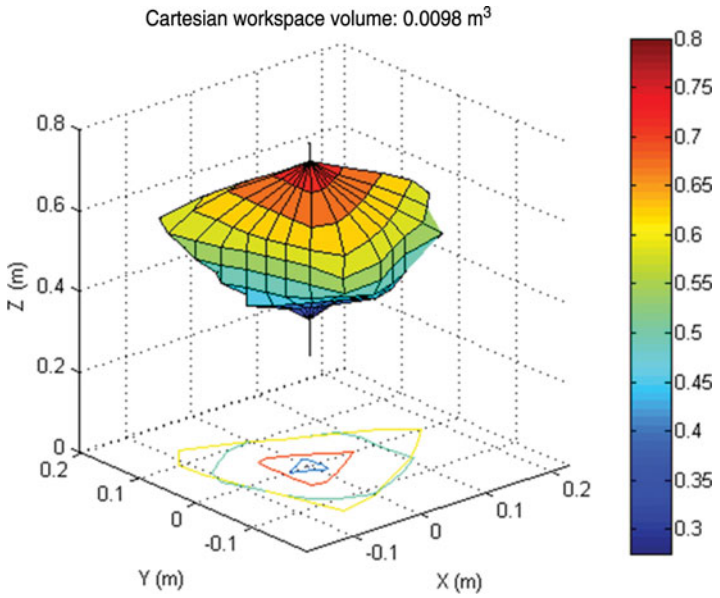


Fig. 3. Cartesian workspace of case study mechanism.

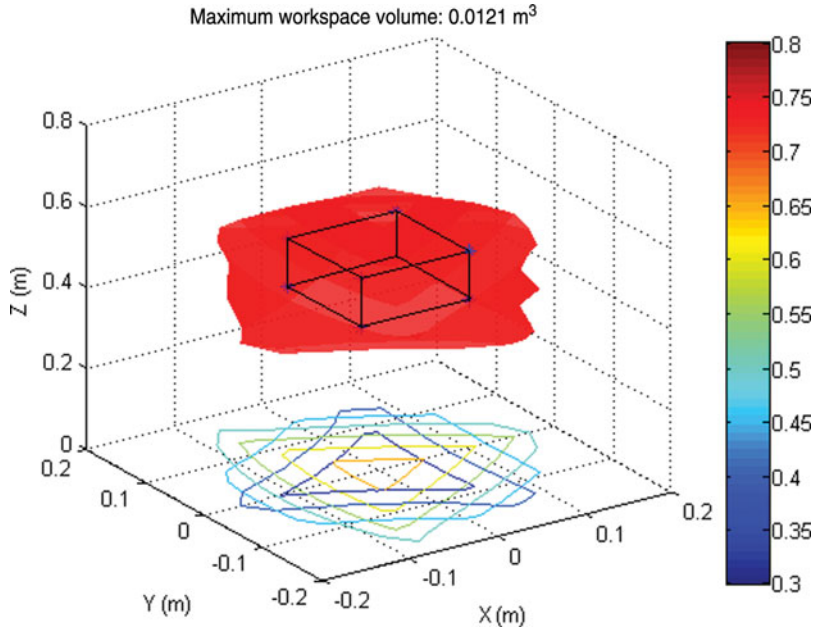


Fig. 4. Optimal Cartesian workspace and associated maximum inscribed cube.

The above equation leads to the following results:

Figure 4 shows the optimum Cartesian workspace and the associated maximum inscribed cube which is calculated by the search algorithm as used by Hosseini and Daniali.[11] The cube volume is 14% of the total Cartesian workspace volume.

4.2. Maximum dexterous Cartesian workspace

Bounding MSV of the Cartesian Jacobian matrix to the minimum desired value, the workspace will be limited to dexterous workspace with high positioning and orienting rates. Accordingly, as the minimum bound increases the minimum desired positioning and orienting rates will increase

https://doi.org/10.1017/S0263574714000861 Published online by Cambridge University Press

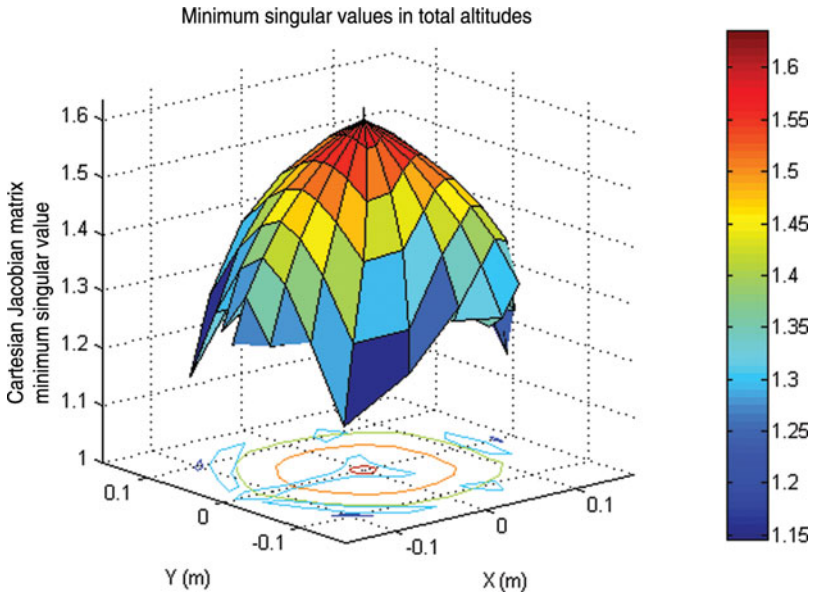


Fig. 5. Minimum singular values variation throughout the Cartesian workspace.

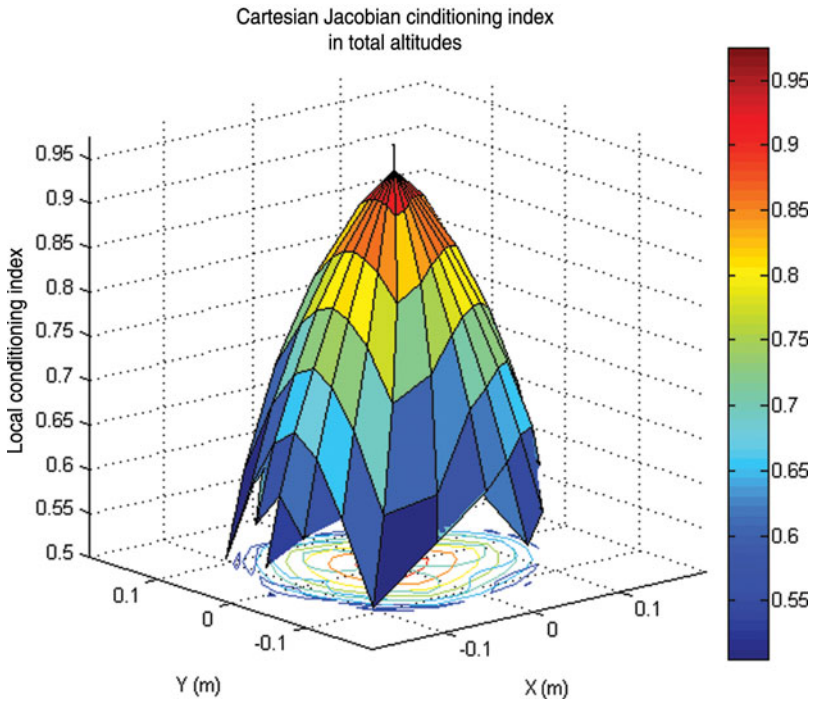


Fig. 6. Local condition number variation throughout the Cartesian workspace.

as well.[11] Figures 5 and 6 illustrate MSV and local condition number as two important indices throughout the workspace for the structure with parameters as depicted in Table III.

Considering 0.6 and 1.3 for the lower bound of local condition number and MSV of the homogenized Jacobian matrix, respectively, the workspace will be restricted to the desired positioning and orienting rates. Importing the mentioned design constraints, for the structure with the parameters of Table III, leads to the workspace as depicted in Fig 7.

Figure 7 illustrates that 76.86% of total Cartesian workspace has the desired positioning and orienting rates. Moreover, the maximum inscribed cube in this sub-workspace is a cube with length

https://doi.org/10.1017/S0263574714000861 Published online by Cambridge University Press

Table III. Optimum structure to achieve maximum Cartesian workspace.

No. of iteration	Workspace volume (m^3)	Cube volume (m^3)	d (m)	r_b (m)	r_a (m)
51	0.0121	0.0017	0.2	0.5	0.22

Table IV. Optimized structure to achieve maximum semi-cubic Cartesian workspace.

No. of iteration	Workspace volume (m^3)	Cube volume (m^3)	d (m)	r_b (m)	r_a (m)
51	0.0113	0.0018	0.211	0.5	0.2

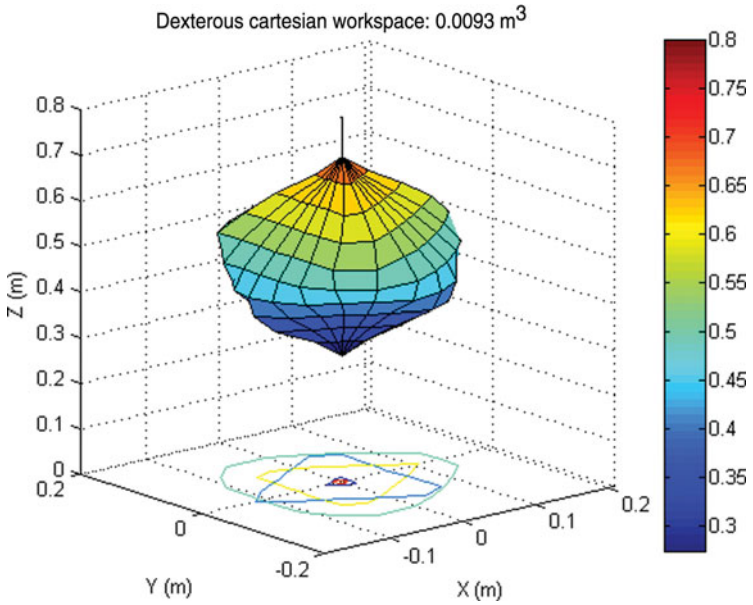


Fig. 7. Sub-workspace with desired positioning and orienting rates.

equal to 109.1 mm. So, the cube occupies just 13.59% of this volume. Thus, this workspace should be optimized by considering dexterity constraints as follows:

$$V^* = \text{Max}(V(r_a, r_b, d)),$$

subject to

$$\begin{aligned} &1.\ \ 0.2 < r_a < 0.3, 0.3 < r_b < 0.5, 0.02 < d < 0.7 \\ &2.\ \ \text{LCI} >= 0.6,\ \ \text{Min}\, SV >= 1.3. \end{aligned} \tag{17}$$

The optimal result is given in Table IV.

Dexterous Cartesian workspace is illustrated in Fig. 8. The maximum inscribed cube is 16.03% of workspace volume.

5. Conclusion

The positioning and orienting rates in parallel robots are functions of its EE position. Despite the importance of workspace volume in the design process of parallel robot, it is necessary to consider dexterous workspace. For the dexterous workspace, rapid positioning can be reached in high-speed applications. Here, we applied minimum singular values and LCI of a new dimensional homogeneous Jacobian matrix called Cartesian Jacobian matrix, as well as the positioning rate indices. Additionally, we used the GA method which led to the optimum structure with optimal workspace,

https://doi.org/10.1017/S0263574714000861 Published online by Cambridge University Press

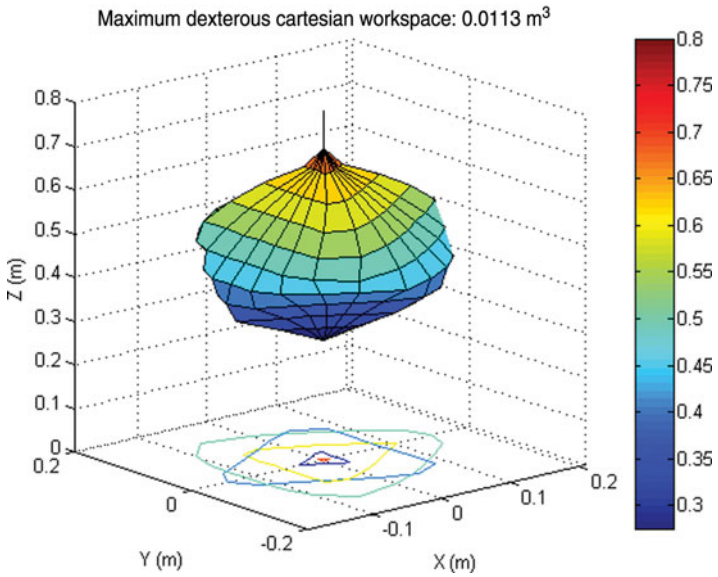


Fig. 8. Maximum dexterous Cartesian workspace.

dexterous workspace size, and regular shape, separately. This research shows that in order to have the maximum dexterous shape and size of a Tricept parallel robot, with machine tool application, the middle universal joint position plays an important role in the problem. Moreover, the optimal cubic dexterous workspace obtained in the structure within the middle passive universal joint, is not connected to the moving platform.

References

1. J.-P. Merlet, *Parallel Robots* (Springer, Dordrecht, 2006).
2. O. Masory and J. Wang, "Workspace evaluation of Stewart platforms," *Adv. Robot. J.* **9**(4), 443–461 (1995).
3. J. A. Carretero, R. P. Podhorodeski, M. A. Nahon and C. M. Gosselin, "Kinematic analysis and optimization of a new three degree-of freedom spatial parallel manipulator," *J. Mech. Des.* **122**(1), 17–24 (2000).
4. T. Yoshikawa, "Manipulability of robotic mechanisms," *Int. J. Robot. Res.* **4**(2), 3–9 (1985).
5. J. K. Salisbury and J. J.Craig, "Articulated hands: Force control and kinematic issues," *Int. J. Robot. Res.* **1**(4), 4–17 (1982).
6. C. Gosselin and J. Angeles, "A global performance index for the kinematic optimization of robotic manipulators," *ASME Trans. J. Mech. Des.* **113**(3), 220–226 (1991).
7. H. Chen, W. Chen and J. Liu, "Optimal design of Stewart platform safety mechanism," *Chin. J. Aeronautice* **20**(4), 370–377 (2007).
8. J. Ryuand and J. Cha, "Volumetric error analysis and architecture optimization for accuracy of HexaSlide type parallel manipulators," *Mech. Mach. Theory* **38**(3), 227–240 (2003).
9. Y. LI and Q. XU, "Optimal Kinematic Design for a General 3-PRS Spatial Parallel Manipulator Based on Dexterity and Workspace," *The 11th International Conference on Machine Design and Production,* Antalya, Turkey (Oct. 13–15, 2004) pp. 571–584.
10. M. A. Hosseini, H. R. M. Daniali and H. D. Taghirad, "Dexterous workspace optimization of a tricept parallel manipulator," *Adv. Robot.* **25**, 1697–1712 (2011).
11. M. A. Hosseini and H. R. M. Daniali, "Dexterous workspace shape and size optimization of a tricept parallel manipulator," *Int. J. Robot.* **2**(1), 18–26 (2011).
12. F. Ranjbaran, J. Angeles, M. A. Gonzalez-Palacios and R. V. Patel, "The mechanical design of a seven-axes manipulator with kinematic isotropy," *J. Intell. Robot. Syst.* **14**, 21–41 (1995).
13. O. Ma and J. Angeles, "Optimum Architecture Design of Platform Manipulators," *Proceedings of the IEEE International Conference on Advanced Robotics*, Montreal, Quebec, Canada, vol. 2 (Jun. 19–22, 1991) pp. 1130–1135.
14. D. Chablat, Ph. Wenger, S. Caro and J. Angeles, "The ISO-Conditioning Loci of Planar Three DOF Parallel Manipulators," *Proceedings of DETC'2002, ASME Design Engineering Technical Conferences*, Montreal, Quebec, Canada, vol. 1 (Oct. 22, 2002) pp. 129–138.
15. C. M. Gosselin, "The optimum design of robotic manipulators using dexterity indices," *J. Robot. Auton. Syst.* **9**(4), 213–226 (1992).

https://doi.org/10.1017/S0263574714000861 Published online by Cambridge University Press

16. S.-G. Kim and J. Ryu, "New dimensionally homogeneous Jacobean matrix formulation by three end-effector points for optimal design of parallel manipulators," *IEEE Trans. Robot. Autom.* **19**(4), 731–737 (2003).
17. G. Pond and J. A. Carretero, "Quantitative dexterous workspace comparison of parallel manipulators," *Mech. Mach. Theory* **42**(10), 1388–1400 (2007).
18. J. Angeles, "Is there a characteristic length of a rigid-body displacement?" *Mech. Mach. Theory* **41**, 884–896 (2006).
19. I. Mansouri and M. Ouali, "A new homogeneous manipulability measure of robot manipulators based on power concept," *J. Mechatronics* **19**, 927–944 (2009).
20. M. A. Hosseini and H. M. Daniali, "Weighted local conditioning index of a positioning and orienting parallel manipulator," *Sientica Iranica* B **18**(1), 115–120 (2011).
21. K.-E. Neumann, *US patent 4*, 732,525 (Mar. 22, 1988).
22. B. Siciliano, "The Tricept robot: Inverse kinematics, manipulability analysis and closed-loop direct kinematics algorithm," *Robotica* **17**(4), 437–445 (1999).
23. D. Zhang and C. M. Gosselin, "Kinetostatic analysis and design optimization of the tricept machine tool family," *J. Manuf. Sci. Eng.* **124**(3), 725–733 (2002).
24. Y. Lu, Y. Shi and B.Hu, "Solving Reachable Workspace of Some Parallel Manipulators by CAD Variation Geometry," *Proc. Inst. Mech. Eng., Part C, J. Mech. Eng. Sci*. **222**(9), 1773–1781 (2008).
25. Y. Lu, B. Hu and T. Sun, "Analyses of velocity, acceleration, statics, and workspace of a 2(3-SPR) serial-parallel manipulator," *Robotica* **27**(4), 529–538 (2009).

https://doi.org/10.1017/S0263574714000861 Published online by Cambridge University Press